OPEN ACCESS

Side-Reactions of Polyvinylidene Fluoride and Polyvinylidene Chloride Binders with Aluminum Chloride-Based Ionic Liquid Electrolyte in Rechargeable Aluminum-Batteries

To cite this article: Eugen Zemlyanushin *et al* 2024 *J. Electrochem. Soc.* **171** 110507
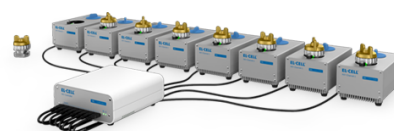
View the article online for updates and enhancements.

Side-Reactions of Polyvinylidene Fluoride and Polyvinylidene Chloride Binders with Aluminum Chloride-Based Ionic Liquid Electrolyte in Rechargeable Aluminum-Batteries

Eugen Zemlyanushin,[1,2,z] Annika Lykka Müller,[1] Tetsuya Tsuda,[2] and Sonia Dsoke[1,3,4,z]

[1]*Institute for Applied Materials (IAM) Karlsruhe Institute of Technology (KIT), Hermann-von-Helmholtz Platz 1, 76344 Eggenstein-Leopoldshafen, Germany*
[2]*Department of Materials Science, Chiba University (CU), 1-33 Yayoi-cho, Inage-ku, Chiba-shi, Chiba 263-8522, Japan*
[3]*Albert-Ludwigs-University Freiburg, Department of Sustainable Systems Engineering (INATECH), Emmy-Noether-Straße 2, 79110 Freiburg, Germany*
[4]*Fraunhofer Institute for Solar Energy Systems, Department of Electrical Energy Storage, Heidenhofstr. 2, 79110 Freiburg, Germany*

Rechargeable aluminum batteries (RABs) use a Lewis acidic aluminum chloride ($AlCl_3$) and 1-Ethyl-3-methylimidazolium chloride (EMImCl) ionic liquid electrolyte. Electrode fabrication often relies on procedures from lithium-ion batteries (LIBs), including the use of Polyvinylidene fluoride (PVdF) as a binder. However, PVdF reacts with $Al_2Cl_7^-$ in the RAB electrolyte, making it unsuitable for new battery types. The literature lacks details on the products formed, changes in the ionic liquid electrolyte, and the implications for electrochemical performance. With potential European Chemical Agency restrictions on per- and polyfluoroalkyl substances (PFAS) by 2025, Polyvinylidene chloride (PVdC) is being explored as an alternative binder. In contact with $AlCl_3$:EMImCl (1.50:1.00) electrolyte, both, PVdF and PVdC transform into amorphous carbon during dehydro-fluorination and dehydrochlorination, respectively, as confirmed by Raman spectroscopy. Furthermore, via ^{19}F-NMR, it is shown that the reaction time between the soaked polymers and the ionic liquid has a significant influence on the newly formed aluminum chlorofluoride complexes. Electrochemical tests of graphite-based electrodes indicate increasing specific capacity of PVdF compared to PVdC with a continuous number of cycles. Amorphous carbon can prevent the disintegration of graphite and enhance conductivity. Furthermore, newly formed AlF_4^- can run a co-intercalation and lead to increasing specific capacity.

Supplementary material for this article is available online

By far, Polyvinylidene fluoride (PVdF) is the most widely used binder material for cathodes in Lithium-Ion Batteries (LIBs).[1] In the case of research for Lithium (Li) alternatives like Sodium (Na)-,[2] Potassium (K)-,[3] Magnesium (Mg)-,[4] Calcium (Ca)-,[5] or Aluminum (Al)-based[6,7] energy storage systems, PVdF is used as binder material as well. The following properties of the fluoropolymer make it almost indispensable as a battery component: Thermal stability, mechanical strength, and chemical resistance. PVdF does not show any reactions in contact with acids, bases, aromatic solvents, and oxidizing agents.[8,9] However, strong bases and organic amines initiate a gradual dehydro-fluorination (DHF), which leads to the formation of hydrofluoric acid (HF) and carbon-carbon sp^2-hybridized double bonds in the polymer chain.[8,10] In the case of the usage of PVdF as a binder material for the positive electrodes in Rechargeable Aluminum Batteries (RABs), several authors report a visible side reaction between the Aluminum chloride ($AlCl_3$)/1-Ethyl-3-methylimidazolium chloride (EMImCl)-based ionic liquid (IL) and the polymer.[11–13] It is possible to see with the naked eye that the mix of the white PVdF powder and the colorless electrolyte turns black very quickly. At this point, it is important to mention that the ionic liquid should be Lewis acidic. This is possible to achieve by mixing a molar ratio of $AlCl_3$ bigger than 1.00 compared to the EMImCl. With such a ratio, for example, 1.10:1.00, 1.30:1.00, 1.50:1.00, or 2.00:1.00, the formation of the acidic $Al_2Cl_7^-$ complex is more favourable (see Eq. 1),[14] which is supposed to be responsible for the reaction with the binder material.[11,15] However, $Al_2Cl_7^-$ is essential to achieve successful electroplating and electro-stripping of the Al negative electrode.

[So far, only Chen et al.[16,17] mentioned the decomposition of the $-CF_2$ group of PVdF and described no effect on the performance of cobalt boride (CoB) cathode material. Smajic et al.[13] reported similar results for reduced graphene oxide dried under supercritical conditions (RGOCPD) used as positive electrode for RABs in ionic liquid electrolyte. A detaching/delamination effect of the active material from the current collector has been observed by Chen et al.[17] due to a swelling effect of PVdF in $AlCl_3$:EMImCl (1.30:1.00) electrolyte. To the knowledge of the authors of this work, in 2015 only Wang et al.[11] reported that PVdF dissolves and partially reacts with the ionic liquid electrolyte which leads to a significant decrease in the electrochemical performance. Therefore, a new binder-free Ni-V_2O_5-based positive electrode was investigated at that time.[11] It is worth mentioning that the used ionic liquid was made of $AlCl_3$ and 1-Butyl-3-methylimidazolium chloride (BMImCl) in the molar ratio of 1.10:1.00. Nevertheless, both kinds of electrolytes form the same two necessary complexes, $AlCl_4^-$ and $Al_2Cl_7^-$. Therefore, the interaction between the polymer binder and the $Al_2Cl_7^-$ is the same. However, until now, no one has uncovered the possible side reaction products of PVdF or has been able to explain the change of color. In the present work, to understand the reaction mechanism, the standard and well-investigated Aluminum-Graphite (Al-C) cell configuration has been used. Graphite is applied as the positive electrode in RABs due to its ability to run reversible intercalation of $AlCl_4^-$ ions. Equations 2 and 3 show the corresponding half-reactions occurring during the charge of an Al-C cell.

$$\text{Negative electrode: } 4Al_2Cl_7^- + 3e^- \rightleftharpoons 7AlCl_4^- + Al \qquad [2]$$

$$xAlCl_3 + EMImCl \rightleftharpoons EMIm^+ + (2-x)AlCl_4^- + (x-1)Al_2Cl_7^- \ (where\ 1 < x \leqslant 2) \qquad [1]$$

$$\text{Positive electrode: } xC + AlCl_4^- \rightleftharpoons C_x(AlCl_4^-) + e^- \qquad [3]$$
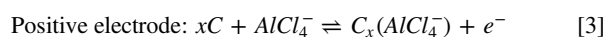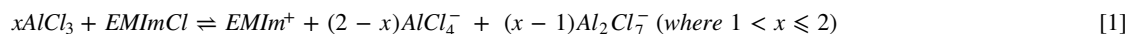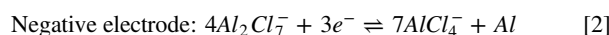
[z]E-mail: eugen.zemlyanushin@kit.edu; sonia.dsoke@ise.fraunhofer.de

For the investigation of the polymer powders and ionic liquid samples, different measurement techniques like FT-IR (Fourier-transform infrared)-, Raman-, and ^{1}H/^{13}C/^{19}F-NMR (nuclear magnetic resonance) spectroscopy have been applied. These techniques have been chosen, because they don't need direct contact with the Lewis acidic ionic liquid electrolyte and therefore prevent damage of devices. In addition, Polyvinylidene chloride (PVdC) was tested under the same conditions to have a direct comparison and to possibly find an alternative for PVdF because the European Chemical Agency (ECHA) could decide to restrict the use of per- and polyfluoroalkyl substances (PFAS) by 2025.[18] Furthermore, the idea is to use a chloride-based material to avoid halogen exchange reactions, the dissolution of the binder, and the resulting detaching of active material from the current collector. Moreover, an alternative slightly Lewis acidic electrolyte made of AlCl$_3$:Urea (1.07:1.00), in which the molar ratio of 1.07 was the minimum amount of AlCl$_3$ to get a fully dissolved and colorless electrolyte, was used to prove that Al$_2$Cl$_7^-$ is responsible for occurring side-reaction.

Materials and Methods

Polyvinylidene chloride ((-CH$_2$CCl$_2$-)n, PVdC, GoodFellow; Polyvinylidene fluoride ((-CH$_2$CF$_2$-)n, PVdF) Solvay; *N*-Methyl-2-pyrrolidone (C$_5$H$_9$NO, NMP), 99.5%, Sigma-Aldrich; Dimethyl sulfoxide (C$_2$H$_6$OS, DMSO), ⩾99.5%, VWR Chemicals; Graphite (C), Mechano-Cap®1P1, H.C. Carbon; Carbon Black (C65), TIMCAL C-NERGY™; Aluminum chloride (AlCl$_3$), 99.999%, Thermo Scientific; 1-Ethyl-3-methylimidazolium chloride (C$_6$H$_{11}$N$_2$Cl, EMImCl), 97% Thermo Scientific; Urea (CH$_4$N$_2$O), ⩾98%, Sigma-Aldrich; ortho-1,2-Difluorobenzene (*o*-C$_6$H$_4$F$_2$), 99%, Apollo Scientific, Aluminum foil (Al), 99.0%, 0.025 mm thickness, GoodFellow; Carbon paper E15 (CP), QuinTech.

All chemicals, carbon paper, and Al-foil have been used as received without any further purification. All air and moisture-sensitive materials, as well as dried electrodes, were stored inside an Argon (Ar) filled Glovebox (MBraun, O$_2$, and H$_2$O < 0.5 ppm). Preparation of AlCl$_3$/EMImCl (1.50:1.00) electrolyte, the assembling/reassembling of Swagelok-type cells, and washing of electrodes or binder sample powders have been always done under an inert Ar atmosphere.

Preparation of AlCl$_3$/urea (1.07:1.00) electrolyte.—Before use, Urea was dried in a Büchi glass oven under vacuum at 100 °C for 6 h and then transferred into the Glovebox. For preparation, 0.82 g AlCl$_3$ (6.12 mmol, 1.07 eq.) and 0.346 g Urea (5.76 mmol, 1.00 eq.) were mixed under stirring. After finishing the addition of both salts, the mixture was heated for 2 h at 60 °C. After, the clear, slightly Lewis acidic[19] electrolyte was allowed to stir at room temperature for 12 h.

Preparation of AlCl$_3$/EMImCl (1.50:1.00) ionic liquid electrolyte.—Inside an Ar-filled Glovebox, 8.00 g (60.00 mmol, 1.50 eq.) AlCl$_3$ and 6.04 g (41.19 mmol, 1.00 eq.) EMImCl were mixed into a vial under stirring. Since the formation of the ionic liquid is a strong exothermic reaction, it is critical to mix both salts very slowly to avoid partly appearing hotspots which can cause electrolyte decomposition. The formation of white smoke/fog indicates that the addition is too fast and should be continued in a much slower way.[20] After completing the mixing process, the ionic liquid was stirred for 12 h. As a result, a clear colorless liquid was obtained.

Electrode preparation.—For the preparation of the PVdF-based electrodes, 90 mass% Graphite (400 mg, 33.30 mmol, 67.96 eq.), 3 mass% C65 conductive carbon (13.30 mg, 1.11 mmol, 2.27 eq.) and 7 mass% of the 10 mass% PVdF binder (311.10 mg, 0.49 mmol, 1.00 eq.), dissolved in *N*-Methyl-2-pyrrolidone (NMP) were used. In the case of the PVdC-based electrodes, 90 mass% Graphite (400 mg, 33.30 mmol, 104.06 eq.), 3 mass% C65 conductive carbon (13.3 mg, 1.11 mmol, 3.47 eq.) and 7 mass% of the 10 mass% PVdC binder (311.10 mg, 0.32 mmol, 1.00 eq.), dissolved in *N*-Methyl-2-

pyrrolidone (NMP) were used. It is important to pay attention to the fact that the calculation of the amount of substance, in mole, and the corresponding equivalent are based on the real amount of pure binder material (31.10 mg) and not the 10% mixed solution. In addition, the calculation is based on the mono unit of the PVdF; M = 64.03 g.mol^{-1} and PVdC; M = 96.94 g.mol^{-1} of the polymer chain. For the preparation of the PVdF binder solution, 1.00 g of PVdF (15.62 mmol, 1.00 eq.) was added slowly under stirring to 10 ml NMP (103.90 mmol, 6.65 eq.). In the case of the preparation of the PVdC solution, 1.00 g PVdC (10.32 mmol, 1.00 eq.) was added slowly under stirring to 10 ml NMP (103.90 mmol, 10.07 eq.). Both, binder solutions were allowed to stir for 12 h before use.

To prepare a slurry, Graphite, and C65 conductive carbon were mixed and ground in a mortar for ten minutes before the powders were further dry mixed for two minutes at 1000 rpm (revolutions per minute) by using a speedmixer (DAC 150.1 FVZ SPEEDMIXER™ from Hauschild). Afterward, 170 µl of DMSO were added as a wetting agent to obtain a thick paste and mixed again for two minutes at 1000 rpm. Further, 2 more drops of DMSO were added and mixed at 2500 rpm for two minutes. The last step was repeated until the slurry became a thick paste. As a next step, the mixture was sonicated for ten minutes and mixed at 2500 rpm for ten minutes to get a homogenous distribution of the components. Then, the corresponding binder solution was added and mixed at 800 rpm for an additional ten minutes. The obtained slurry was coated via the Doctor Blade technique on carbon paper with a wet thickness of 200 µm. The coated carbon paper was dried under ambient conditions inside a fume hood for 12 h. After that, the coating was dried in a Binder oven at 65 °C for 8 h. Then, electrodes were punched out to 12 mm diameter discs with a GN-CP20 punching machine from the Gelon group and dried in a Büchi B-585 glass oven under vacuum at 110 °C for 12 h. Finally, the electrodes were transferred into a Glovebox. The average mass loading for PVdF electrodes is 5.22 ± 0.43 mg.cm^{-2} and for PVdC 5.63 ± 0.48 mg.cm^{-2}.

Cell assembling and electrochemical characterization.—All electrochemical measurements have been done with a two-electrode configuration using a Swagelok-type cell, whereby the rods are made of Tungsten (W) to avoid any side reactions with the Lewis acidic electrolyte. To assemble the cell, first, a 12 mm in diameter Al-foil (1.131 cm^2, punched out with a Turnus bracket hollow) was placed on one rod screwed to the PTFE Swagelok body. On top of the Al-foil, a 13 mm in diameter glass-fiber separator (Whatman, GF/A) was placed. The punching of the separator has been done with a GN-CP20 punching machine from the Gelon group. This separator was allowed to get soaked with 200 µl of ionic liquid electrolyte before a second separator was placed into the cell-body part. An additional amount of 100 µl of electrolyte was added to wet the second separator too. Finally, a weighted PVdF- or PVdC-based graphite electrode was inserted before the Swagelok cell was closed. All electrochemical tests were carried out using a VMP3 multichannel potentiostat/galvanostat from Bio-logic Science Instrument (France), equipped with the EC-Lab®, software version V11.43. Furthermore, all test cells were placed in a climate chamber at a constant temperature of 25 ± 1 °C. Galvanostatic charge/discharge cycling with potential limitation (GCPL) experiments were performed in a potential window of 0.30–2.30 V vs Al with a current of 20 mA.g^{-1}. Cyclic voltammetry (CV) was performed with a scan rate of 0.20 mV.s^{-1} from 0.30–2.30 V vs Al. The average open-circuit voltage (OCV) of the assembled cells was ∼1.60 V. Electrochemical data evaluation was done with OriginPro 2023 from OrginLab.

Characterization techniques.—Raman spectroscopy was done with a Raman spectrometer (LabRam Evolution HR, HORIBA Jobin Yvon) with 633 nm laser excitation.

Fourier-transform infrared (FT-IR) spectra were recorded by a Bruker Tensor 27 FT-IR spectrometer.

Nuclear magnetic resonance (NMR) spectroscopy has been recorded with a Bruker Avance 400 spectrometer. For measuring
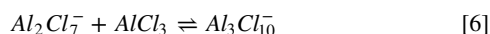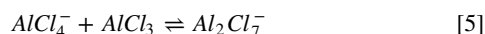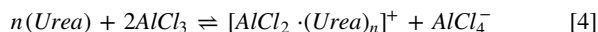
^{1}H, ^{13}C, and ^{19}F the following frequencies were used: 400 MHz, 101 MHz, and 376 MHz, respectively. Data evaluation was done with MestReNova from Mestrelab Research, software version 14.1.2-25024.

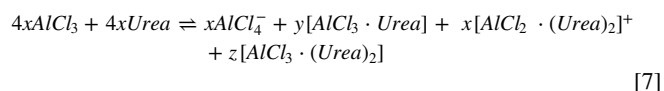All raw data have been plotted with OriginPro2023 from OriginLab.

Results and Discussion

According to the literature, the side reactions of the PVdF could be explained by two different approaches: First, the above-mentioned interaction with $Al_2Cl_7^-$ [11,15] or the influence of the EMImCl salt to achieve a phase transformation of a non-polar α-PVdF toward an electroactive, highly polar β-PVdF.[21] The phase transformation can occur because of the interaction of the positive charge of the imidazolium ring's nitrogen with the PVdF's fluoride atoms, and the interaction of $AlCl_4^-$ anions with the PVdF's hydrogen atoms. Both interactions lead to rearranging the F- and H-atoms of the PVdF as shown in Fig. 1. This comparison has been done with a similar system based on the interaction between PVdF, EMIm$^+$, and PF$_6^-$.[22]

To make sure which component of the ionic liquid is responsible for the side reaction, including the color change, the PVdF and PVdC binders were soaked in $AlCl_3$/ Urea (1.07:1.00) electrolyte. The $AlCl_3$/Urea electrolyte does not contain any EMImCl but forms $Al_2Cl_7^-$ complex, like it is shown in Eqs. 4.[23–26] The ratio of 1.07:1.00 has been chosen because it is the first ratio to obtain a clear completely dissolved electrolyte.

$$n(Urea) + 2AlCl_3 \rightleftharpoons [AlCl_2 \cdot (Urea)_n]^+ + AlCl_4^- \qquad [4]$$

$$AlCl_4^- + AlCl_3 \rightleftharpoons Al_2Cl_7^- \qquad [5]$$

$$Al_2Cl_7^- + AlCl_3 \rightleftharpoons Al_3Cl_{10}^- \qquad [6]$$

In Eq. 4, n is the coordination number of Urea, which depends on the molar ratio between $AlCl_3$ and Urea. In the case of preparing a neutral system of $AlCl_3$:Urea (1.00:1.00), several $[AlCl_v \cdot Urea_w]^{u+}$ complexes are formed, but no $Al_2Cl_7^-$ is obtained (Eq. 7).[23,25,26]

$$4xAlCl_3 + 4xUrea \rightleftharpoons xAlCl_4^- + y[AlCl_3 \cdot Urea] + x[AlCl_2 \cdot (Urea)_2]^+ + z[AlCl_3 \cdot (Urea)_2]$$
$$[7]$$

The values of x, y, and z were determined to be 1.00, 2.49, and 0.03, respectively, for the species shown in Eq. 7.[23] In our experiment, both, PVdF and PVdC, change their color from white and light brown to black, respectively, during soaking in $AlCl_3$:Urea (1.07:1.00). Since even the slightly Lewis acidic non-EMImCl containing electrolyte leads to the same color change as the $AlCl_3$/EMImCl (1.50:1.00) ionic liquid, it is confirmed that the side reactions and color change are related to the $Al_2Cl_7^-$ complex. The same soaking test was done for PVdF and PVdC using the

$AlCl_3$/EMImCl electrolyte and both polymers turned black (Fig. S1). To separate the liquid from the binder powders, a syringe filter was used. The residual ionic liquid was removed by washing the powders with 1,2-Difluorobenzene before drying at 60 °C under vacuum for 6 h. The residual dark compound was investigated without any further treatment. First, FT-IR measurements of the pristine PVdF and PVdC (Figs. 2A and 2B) were performed and compared with soaked binders (Figs. 2C and 2D). For easier demonstration of the result, the soaked materials are called s-PVdF and s-PVdC. In the case of pristine PVdF, it was possible to assign all vibrational modes (Table S1) of α-PVdF (main phase) and β-PVdF (side-phase) according to the literature.[27–32] The same analysis was done with the PVdC.[33–37] The FT-IR spectra confirm that PVdF has no impurities while PVdC shows unexpected additional bands at 1745 cm^{-1} and 1636 cm^{-1} (marked with an asterisk). Both bands result from an unsaturated carbonyl (C=O) impurity, which is also responsible for the yellowish/light brown color of the usually colorless PVdC powder.[36] Two suitable explanations for this impurity can be given as follows: (I) During the synthesis of PVdC some additives like plasticizers[38] are added and remain in the final product; (II) Chlorinated polymers like polyvinyl chloride (PVC) or PVdC are sensitive to run photooxidation reactions.[35] Figures 2C and 2D shows the FT-IR spectra of s-PVdF and s-PVdC after the reaction with the electrolyte. For comparison, possible products arising from radiation, heating, and/or used strong bases like NaOH/KOH dehydrofluorinated PVdF have been considered. In addition, one publication that demonstrated an FT-IR of PVdF after soaking in $AlCl_3$/EMImCl (1.30:1.00) electrolyte[39] was taken into account. The FT-IR spectra of s-PVdF (Fig. 2C) show four main differences, compared to the pristine PVdF one. First, the dominant bands at 2560–3725 cm^{-1}, 1639 cm^{-1}, 1569 cm^{-1} and 1458 cm^{-1} are visible. At first sight, a dehydrofluorination (DHF) of the binder material was taking place in contact with the ionic liquid. In the case of a successful DHF, additional carbon-carbon double bands appear at 1639 cm^{-1} and 1569 cm^{-1}.[31,40–42] In addition, the corresponding -CF$_2$-based bands become weaker and lower in intensity, which would indeed lead to the formation of C=C bonds and the release of hydrofluoric acid (HF). However, the bands at 3725–2560 cm^{-1} and 1458 cm^{-1} indicate that still EMIm$^+$/AlCl$_4^-$ is inside the sample. The broad huge band is based on the interaction of C–H symmetric/ asymmetric stretching of the alkyl chains, which is causing the signal at 1458 cm^{-1} as well, N–H stretching of the amide and probably O–H stretching, which can interact with chloride ions.[43] Since the washing process was not enough, or the EMIm$^+$/AlCl$_4^-$ is stuck inside the PVdF matrix, several important bands of EMIm$^+$ are overlapping with DHF-PVdF, therefore it is hard to say if the DHF was at least partly occurring. All overlapping bands of s-PVdF and EMIm$^+$ are listed in Table S3, which are based on several reports about EMImCl-based systems.[43,44] Especially the band at 1569 cm^{-1} can lead to a misinterpretation since the signal can appear because of O–H deformation or carbon-carbon double bonds caused by DHF[45] but at the same time, it can be assigned as the C=C
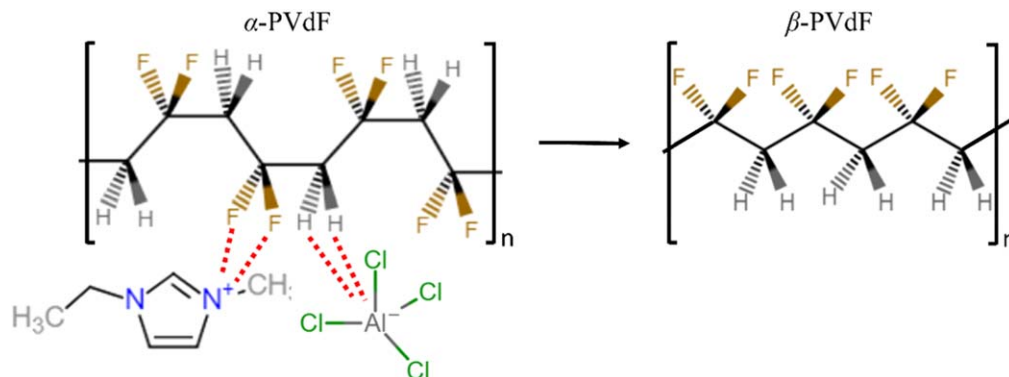

Figure 1. Schematic illustration of the phase transformation of α-PVdF into β-PVdF due to the interaction with EMIm$^+$ and AlCl$_4^-$.
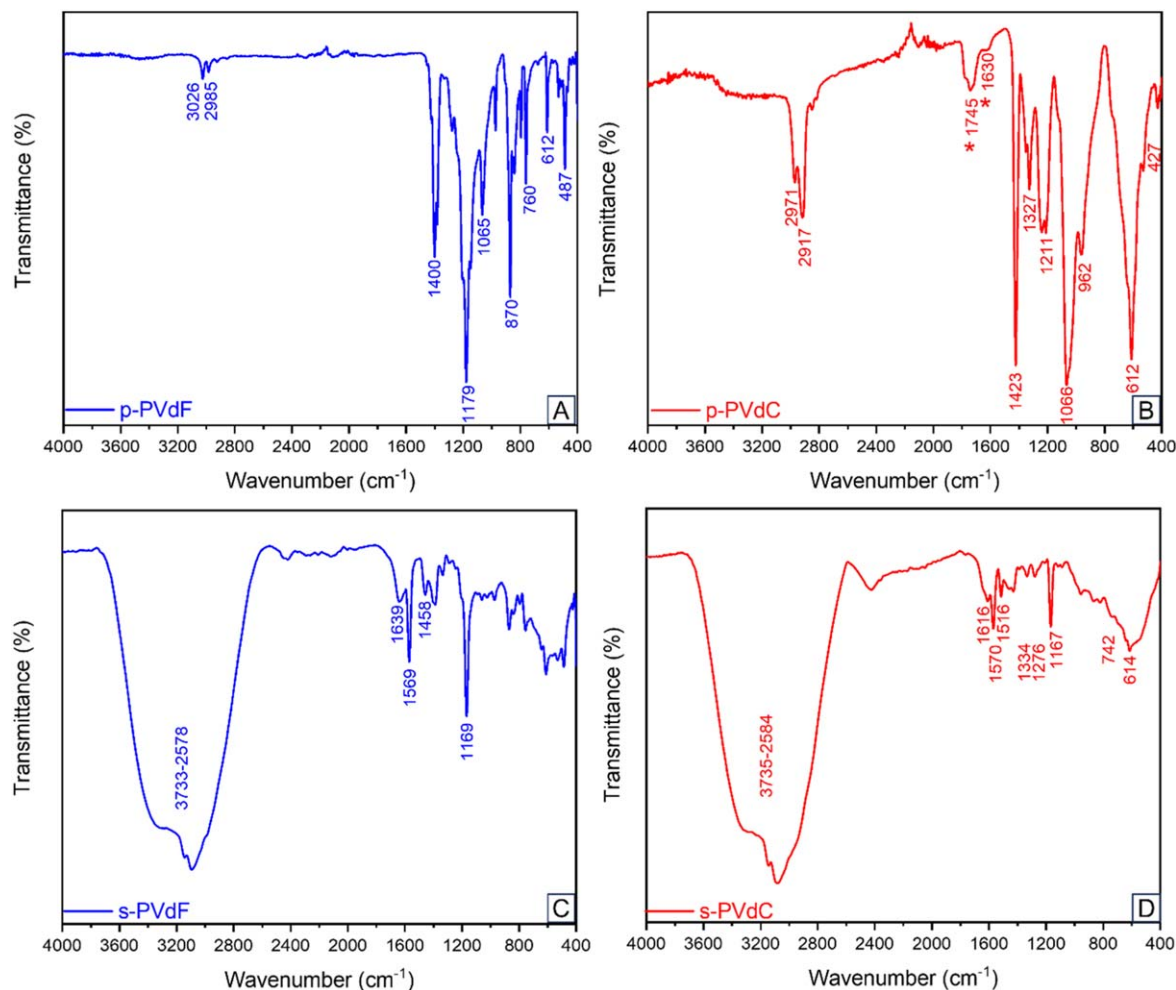
Figure 2. Fourier-transform infrared (FT-IR) spectrograms of (pristine) p-PVdF (A) and p-PVdC (B) powders and soaked in AlCl₃:EMImCl s-PVdF (C) and s-PVdC (D).

asymmetric stretching vibration of the imidazolium ring.[44,46] The same results have been obtained with s-PVdC (Fig. 2D). Only the broad and vanished area between 1050–400 cm^{-1} implies a dehydrochlorination (DHC) reaction.[36,47,48] To overcome the problem of overlapped signals of s-PVdF and s-PVdC with IR-active modes of EMImCl, Raman measurements have been done.

Figure 3C shows the Raman spectra of the s-PVdF. The Raman results indicate the formation of amorphous carbon after contact with the Lewis acidic AlCl₃:EMImCl ionic liquid electrolyte. After sample immersion, typical Raman broad signals for amorphous carbon at 1580 cm^{-1} and 1342 cm^{-1} are present,[49–51] while other Raman bands from the pristine material are not visible anymore (Fig. 3A). The conclusion is that the DHF, caused by interaction with Al₂Cl₇$^-$, leads to the carbonization of PVdF. The formation of pure carbon would also explain the color change of the colorless powder, as well as, of the electrolyte from transparent/yellowish to black. In addition, the vibration mode at 2200 cm^{-1} is an indication of the formation of polyyne, which has been reported to be typical for the dehydrohalogenation of halogens-containing polymers.[52,53] A similar result is obtained for s-PVdC, whereby the D- and G bands are slightly shifted to lower wavenumbers (Fig. 3D). The corresponding signals are located at 1485 cm^{-1} and 1107 cm^{-1}. The Raman spectra of pristine PVdC (Fig. 3B) were measured after dissolving the chloride-based binder material in acetone because the pure material was impossible to measure. The pristine material shows huge differences from the literature spectra of Xiao et al.[35] One possible explanation could be a structural change by dissolving in acetone. On the other hand, maybe the spectra differ because of

the decomposed PVdC surface caused by UV. As a result, DHC can occur and intern crosslink products can be formed. One indication of an impurity is given by the carbonyl group, measured in the FT-IR. The same group activity can be identified by Raman spectroscopy. Taking into account that the D- and G-bands are shifted after reacting with the IL, it can be assumed that the PVdC changed. Streletskiy et al.[51,54] investigated the DHC of PVdC-PVC and obtained a similar Raman band shift. This is an indication that the used PVdC formed some dechlorinated sequences in the polymer chain, which caused a longer sp^2-carbon hybridization bond compared to pure PVdC.[54,55] Moreover, vibration modes at 2200 cm^{-1} appear because of the formed carbon-carbon sp triple bond, the so-called polyyne.[54]

On the other hand, Niino and Yabe[56] obtained the same Raman signals for dehydrochlorinated PVdC, via photo-irradiation, but unfortunately, they don't show Raman spectra of the pristine material, which could show the same kind of degradation as presented in this work. All results indicate that EMIm$^+$/AlCl₄$^-$ always remains in the PVdF polymer matrix and that a DHF and DHC for PVdF and PVdCl, respectively, occurs. Further investigations via NMR have been done to understand the influence of formed HF and HCl on the electrolyte and the impact of these binders on the electrochemical performance of an Aluminum-Graphite cell. In the case of the ^{19}F-NMR of the ionic liquid after soaking PVdF powder (Fig. 4A) for 1 h, two peaks at -155.40 ppm and -158.15 ppm can be observed.

The chemical shifts at -155.40 ppm and -158.15 ppm belong to aluminum fluoride and aluminum chlorofluoride (ACF) complexes.
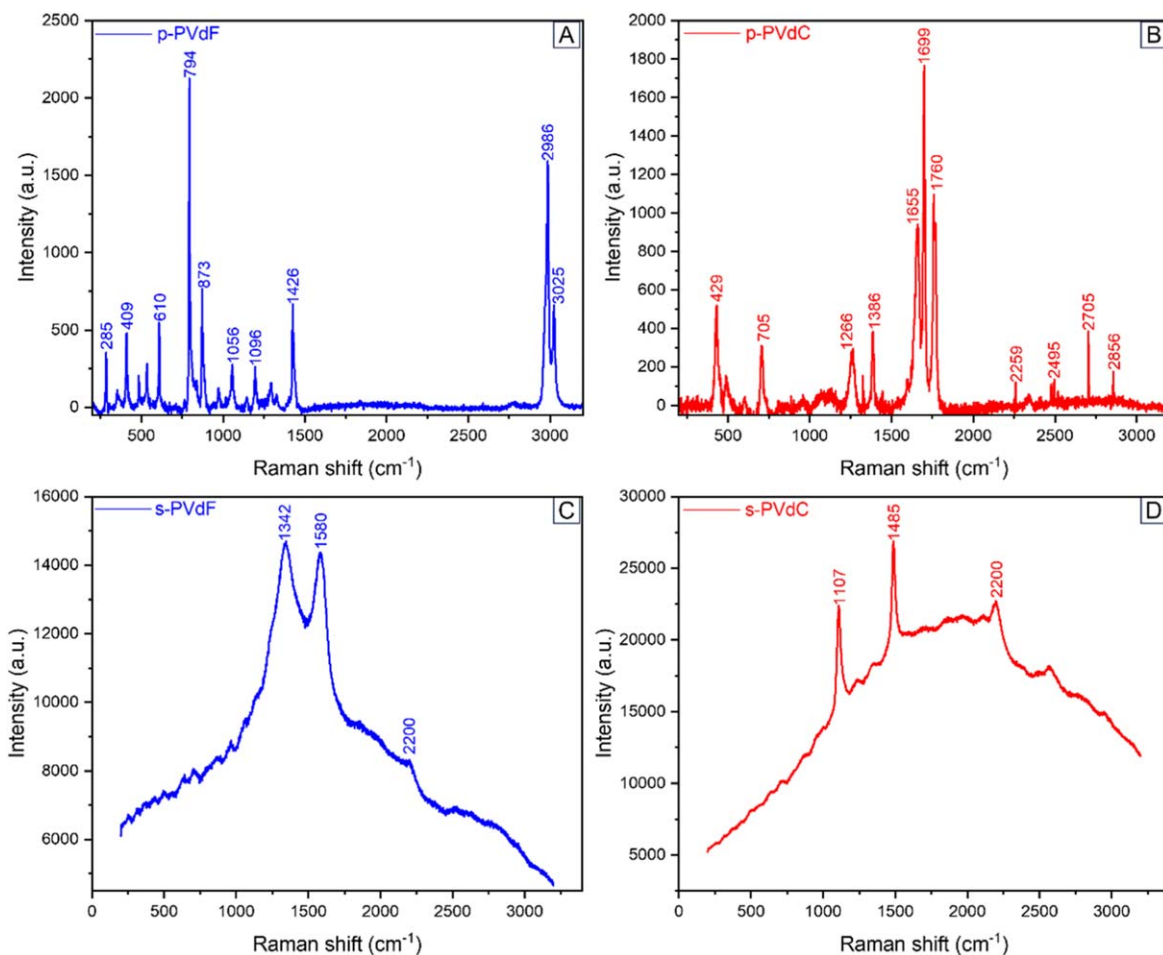
Figure 3. Raman spectra of (pristine) p-PVdF (A) and p-PVdC (B) powders. Furthermore, in $AlCl_3$:EMImCl ionic liquid soaked s-PVdF (C) and s-PVdC (D).
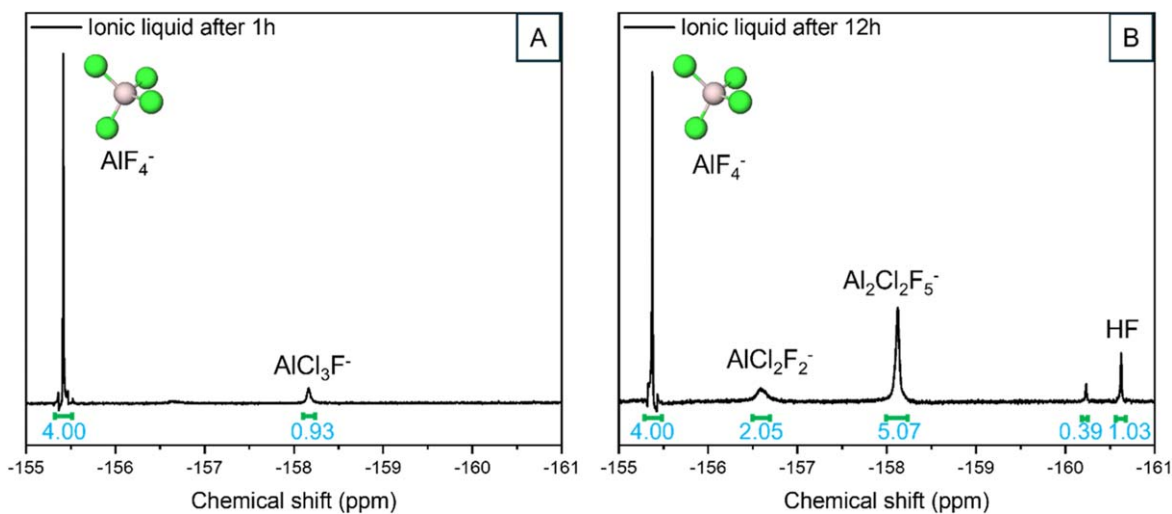

Figure 4. ^{19}F-NMR (nuclear magnetic resonance) spectroscopy of ionic liquid electrolyte (black liquid) after soaking PVdF for 1 h (A) and electrolyte soaked for 12 h (B).

Regarding the report of Bodor et al.[57,58] a less negative chemical shift in the ^{19}F-NMR is related to a complex with higher fluoride content. Therefore, the peaks around −155.40 ppm appear because of the presence of AlF_4^-. The chemical shift at −158.15 ppm should belong to $AlCl_3F^-$ ACF. After 1 h, the DHF of the PVdF polymers leads to halogen exchange of the ionic liquid electrolyte. After soaking PVdF for 12 h (Fig. 4B), the black ionic liquid was measured again. Besides the AlF_4^- signal around −155.36 ppm and the peak at −158.11 ppm,

three additional signals at −156.59 ppm, −160.22 ppm (unknown), and −160.61 ppm were obtained. However, the chemical shift at −158.11 ppm does not anymore belong to the $AlCl_3F^-$ ACF complex. With further soaking time, the DHF of the PVdF binder has increased to the level that HF at −160.61 ppm can be detected. Formed HF and ACF can encourage further and faster DHF, which results in the formation of $AlCl_2F_2^-$ out of $AlCl_3F^-$ and a downshift to − 156.59 ppm. The downshift takes place due to an additional fluoride-chloride
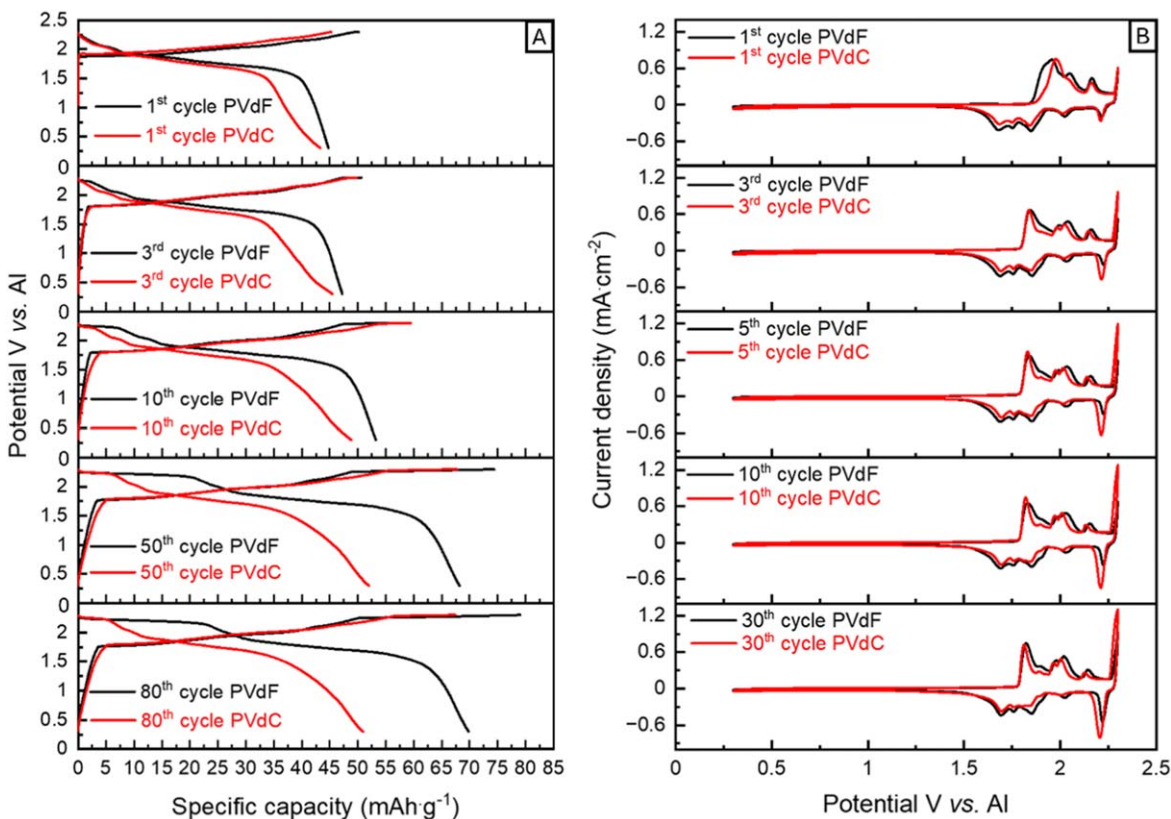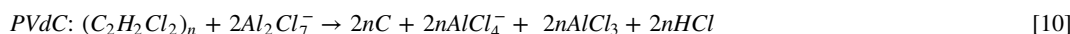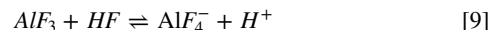
Figure 5. (A) Galvanostatic cycling with potential limitation (GCPL) in the potential window of 0.30 V–2.30 V at a current density of 20 mA.g^{-1} of PVdF- and PVdC-based graphite positive electrodes at different cycle numbers. (B) Corresponding cyclic voltammograms (CVs) with a scan rate of 0.20 mV.s^{-1} at different cycles.

exchange. Since $AlCl_2F_2^-$ is still a symmetric molecule with the same chemical- and magnetic environment of both fluoride atoms, a singlet ^{19}F-NMR is detected. According to this trend of showing a downshift with higher fluoride atoms, the newly formed $Al_2Cl_2F_5^-$ complex should be detected below the chemical shift of ∼-155 ppm (AlF_4^-).

decrease because of the loss of $Al_2Cl_7^-$ required to produce amorphous carbon, HF, HCl, $AlCl_2F_2^-$, $Al_2Cl_2F_5^-$, $AlCl_4^-$, and AlF_4^-. AlF_4^- is considered to be a result of the equilibrium of formed AlF_3 and HF.[57] The proposed initial reaction equation for PVdF and PVdC is shown in Eqs. 8, respectively.

$$PVdF: 2(C_2H_2F_2)_n + nAl_2Cl_7^- \rightarrow 4nC + nAlF_3 + nAlCl_4^- + nHF + 3nHCl \qquad [8]$$

However, one of the $Al_2Cl_2F_5^-$ fluorine atoms serve as a bridge between the two $AlClF_2$-parts. Otherwise, the signal would not be a singlet due to the different chemical- and magnetic environments of all

$$AlF_3 + HF \rightleftharpoons AlF_4^- + H^+ \qquad [9]$$

$$PVdC: (C_2H_2Cl_2)_n + 2Al_2Cl_7^- \rightarrow 2nC + 2nAlCl_4^- + 2nAlCl_3 + 2nHCl \qquad [10]$$

the other fluorine atoms and the whole complex would not get an upshift. The upshift is possible because of a more shielded environment of the $Al_2Cl_2F_5^-$ complex.[59] This would be comparable with the $AlCl_3Br^-$ and $Al_2Cl_6Br^-$ (bromine atom is bridging) complexes, which have been used for aluminum-sulfur and aluminum-selenium batteries.[60,61] Moreover, by increasing the soaking time the DFH and the hydrolyzation to HF are more favorable. ^1H- and ^{13}C-NMR measurements of the black ionic liquid electrolyte confirm that EMImCl does not participate in the side reaction with the PVdF. The spectra of fresh and black electrolytes are shown in Figs. S2A–S2D, respectively. Based on the NMR and Raman results, PVdF is considered to be a precursor carbon source. With the progressive decomposition, the ratio of $AlCl_3$:EMImCl should

After studying the decomposition product of PVdF and PVdC in contact with Lewis acidic ionic liquid electrolyte, galvanostatic cycling with potential limitation (GCPL) and cyclic voltammetry (CV) measurements have been done. The cells consist of positive electrodes made of graphite prepared with PVdF and PVdC binder materials and pure Al-foil as the negative electrode. Figure 5A, shows the GCPL of PVdF- and PVdC-based graphite electrodes at a current density of 20 mA.g^{-1}. In both cases, the initial discharge capacity of circa 45 mAh.g^{-1} is quite low but increases with further cycles. Please note that the normalization of the capacity has been done only on the amount of graphite. After 80 cycles, the PVdF-based cell reaches a discharge capacity of ∼70 mAh.g^{-1} (average coulombic efficiency (CE): ∼92% after 80 cycles) while the PVdC

electrode extends to ~50 mAh·g^{-1} (average CE: ~77% after 80 cycles). In the case of the PVdF-based electrodes, the specific capacity has been reported to be in the range of 70–80 mAh.g^{-1}.[62] The increase in capacity with further cycles has been described already for several different kinds of graphite-based cathode materials. For example, Elia et al.[63] reported a rising capacity for pyrolytic graphite (PG), and Mukundan et al.[64] for natural graphite (NG). Elia,[63] Mukundan,[64] and Huang[65] explain the increase of the capacity with further cycle number by the increase of the *d*-spacing of the graphite layers. By this, the reversible intercalation of the AlCl$_4^-$ anions can be improved, which results in a higher capacity and enhanced rate capability.

It is expected that the capacities of both, PVdF and PVdC-based materials would be relatively low because of the chosen high wet thickness of 200 μm (dry thickness: 238 nm). Huang et al.[65] reported that in AlCl$_3$-based RABs, a high graphite loading leads to lower capacity because the higher volume of graphite hinders the smooth diffusion of AlCl$_4^-$ into the host material. Just for comparison, Appiah et al.[66] figured out that the optimal thickness of a graphite electrode, made of 90% graphite mixed with 10% PVdF binder, in an AlCl$_3$:EMImCl ionic liquid electrolyte system is 50 μm. Moreover, a greater thickness increases the diffusion length of AlCl$_4^-$ and prevents complete deintercalation.[66] By this, the concentration of the AlCl$_4^-$ in the ionic liquid electrolyte decreases and the remaining active species inside the graphite layers hinder intercalation pathways. Consequently, the charge/discharge capacities become lower. In addition, initial cycles count as the activation phase of the graphite during the intercalation of AlCl$_4^-$. During this phase, the specific charge capacity increases while the specific discharge capacity decreases due to irreversibly trapped AlCl$_4^-$ anions.[64] For both materials, the CVs (Fig. 5B) show similar current density as well as stability, which is consistent with the results of Wei et al.,[67] who compared graphite and graphite/amorphous carbon RABs based on AlCl$_3$/EMImCl (1.30:1.00) ionic liquid electrolyte without any changes in redox activity. By this, it is proven that amorphous carbon contributes to improved stability and higher capacity of graphite-based RABs without showing any redox activity.

The difference between PVdF and PVdC-based electrodes is the newly formed AlF$_3$/AlF$_4^-$ species (Eqs. 8 and 9), which could be active as well. XPS results of Chen et al.[17] confirm that the ratio of -CF$_2$ signal of PVdF-based electrodes after getting in touch with AlCl$_3$-based ionic liquid electrolyte, reinforces the ^{19}F-NMR results that the newly formed species is dissolved in the electrolyte. Moreover, in 2023, Yu et al.[68] demonstrated via Raman measurements that 2.5% of added PVdF is enough to destroy AlCl$_4^-$ and Al$_2$Cl$_7^-$ species of the ionic liquid. By this, the ionic liquid electrolyte gets deactivated in its functionality. This could explain why the capacity of the PVdC-based samples is stable at a certain value without relevant variations upon cycling. Captured AlCl$_4^-$ in the graphite host and partly destroyed/deactivated species are replaced by newly formed active species by the side reaction between Al$_2$Cl$_7^-$ and PVdC. On the other hand, PVdF generates new AlCl$_4^-$ as well as AlF$_4^-$, which should be able to intercalate too. Indeed, Matsumoto et al.[69] showed that the intercalation of AlF$_4^-$ occurs successfully in graphite. Moreover, in their study, they suggest a further side reaction of the intercalation product (C$_X$AlCl$_4$) with formed HF (Eq. 11).[70]

Another reason for the increase of capacity with further cycle numbers could be caused by the fact that electrochemically inactive binder materials act like precursors for generating amorphous carbon. Amorphous carbon has been shown by Wei et al.[67] to be able to protect the graphite from disintegration and, therefore, contribute to the improvement of the cycling stability of RABs. Moreover, amorphous carbon can enhance the surface area and increase the conductivity.[72] This is probably the reason why many researchers still use PVdF as a binder despite the side reaction with the ionic liquid electrolyte. Without amorphous carbon, pure graphite electrodes showed in AlCl$_3$/EMImCl (1.30:1.00) electrolyte a lower initial increase of the specific capacity and a faster capacity decay.[67] Compared to PVdF, one major weak point of the PVdC binder must be taken into account; the binding effect of PVdC is noticeably worse. After preparing the electrodes, it was very difficult to handle the PVdC-based graphite electrode without damaging the surface because of the lack of cohesion between the active material and the carbon paper current collector. Since the contact of graphite to the current collector was very weak, the detaching effect (Figs. S3A–S3H) during cycling can explain the very low coulombic efficiency of ~77% of PVdC, compared to ~92% of PVdF.

Conclusions

In this work, the side reactions of PVdF and PVdC binder materials for RABs have been investigated. Both polymers show the same kind of interaction with the Lewis acidic AlCl$_3$:EMImCl (1.50:1.00) ionic liquid. The used electrolyte forms two active species, AlCl$_4^-$ and Al$_2$Cl$_7^-$ while Al$_2$Cl$_7^-$ is responsible for the dehydrofluorination (DHF) and dehydrochlorination (DHC) of PVdF and PVdC, respectively. At the same time, the EMIm$^+$ counter cation does not show any changes and therefore does not participate in the side reactions with the binder materials. As a result of DHF and DHC, the polymer binder changes to an amorphous carbon compound, by forming sp^2 carbon hybridization, and possibly sp polyyne. Formed amorphous carbon can protect the graphite from disintegration and, therefore, contribute to the improvement of the cycling stability of RABs without showing any redox activity. Furthermore, amorphous carbon can increase the surface area of the electrode and improve the conductivity. Moreover, cross-link reactions between the polymer chains are also possible as ring-closing reactions because of the exothermic reaction between Al$_2$Cl$_7^-$ and the polymers as well as the great ability of AlCl$_4^-$ to initiate such reactions. In the case of PVdF, the two typical D- and G bands of amorphous carbon (1580 cm^{-1} and 1342 cm^{-1}) have been observed, while PVdC shows a slight shift to lower wavenumber (1485 cm^{-1} and 1107 cm^{-1}). This Raman shift is caused by a shorter average carbon-carbon bond of the final product of PVdC, which is a further indication of the formed sp carbon hybridization. In addition, ^{19}F-NMR measurements of ionic liquid electrolyte after soaking PVdF for 1 h, validate the formation of AlF$_4^-$ and AlCl$_3$F$^-$molecules. After a soaking time of 12 h, AlF$_4^-$, AlCl$_3$F$_2^-$, Al$_2$Cl$_2$F$_5^-$, and HF were detected. Both binder materials, form during the DHF and DHC reactions AlCl$_4^-$, HF, and HCl, respectively. The generated acids enable a further, even easier DHF and DHC reaction. Electrochemical tests show that PVdF is a better binder material than PVdC for graphite. Both, the capacity and coulombic efficiency of a graphite-based electrode are noticeably better by using PVdF as a binder. The reason for that could be the additional AlF$_4^-$-active species which can intercalate into the graphite host.

$$C_x AlCl_{4\,(s)} + 4HF_{\,(l)} \rightarrow (x - 0.25)C_{\,(s)} + AlF_{3\,(s)} + 4HCl_{\,(g)} + 0.25CF_{4\,(g)} \qquad [11]$$

In that case, the formed AlF$_3$ can further react with HF to produce AlF$_4^-$, as shown in Eq. 9. Wang et al.[71] even predict that the use of AlF$_4^-$ as active intercalating species of RABs will lead to larger cathode-specific capacity, higher voltage, and higher rate capability.

Furthermore, the mechanical instability, caused by the lack of cohesion between graphite and carbon paper current collector, of PVdC-based electrodes makes investigation and research on it difficult and its commercialization impossible. To sum up, the shown side reactions

cause the formation of amorphous carbon via DHF and DHC and the deactivation of the AlCl$_3$:EMImCl ionic liquid electrolyte. Moreover, formed HF and HCl can cause additional corrosion reactions between the metallic current collector and cell parts, which consequently lead to even more unwanted side reactions.

Acknowledgments

Supplementary Materials

The supporting materials include the following information: Fig. S1 Reaction between PVdF and PVdC with Lewis acidic ionic liquid electrolyte after 1 min, 10 min, and 60 min, respectively. Table S1 Fourier-transform infrared (FT-IR) bands of pristine PVdF and PVdC. Table S2 Overlapping bands of EMImCl in comparison to PVdF and PVdC. Figure S2 ^{1}H-NMR (A) and ^{13}C-NMR (B) of pristine AlCl$_3$:EMImCl ionic liquid electrolyte and ^{1}H-NMR (C) and ^{13}C-NMR (D) of soaked "black" electrolyte, respectively. Figure S3 SEM images of p-PVdF (A, top view; B, cross-section) and cycled PVdF (C, top view; D, cross-section); p-PVdC (E, top view; F, cross-section) and cycled PVdC (G, top view; H, cross-section). The data that support the findings of this study are openly available at the KIT Library: https://doi.org/10.35097/2xq6d1at7a12y5sr.

Author Contributions

Conceptualization: E.Z.; Experiments and analysis: E.Z. and A.L. M.; Investigation and methodology: E.Z., A.L.M., T.T. and S.D.; Supervision: T.T. and S.D.; Writing-original draft: E.Z.; Writing-review and editing: E.Z.; T.T. and S.D. All authors have read and agreed to submit this manuscript.

Funding

ORCID

Eugen Zemlyanushin ⓘ https://orcid.org/0000-0002-1711-726X
Tetsuya Tsuda ⓘ https://orcid.org/0000-0001-9462-8066
Sonia Dsoke ⓘ https://orcid.org/0000-0001-9295-2110

References

1. X. Zhang, X. Ge, Z. Shen, H. Ma, J. Wang, S. Wang, L. Liu, B. Liu, L. Liu, and Y. Zhao, *New J. Chem.*, **45**, 9846 (2021).
2. S. L. Chou, Y. Pan, J. Z. Wang, H. K. Liu, and S. X. Dou, *Phys. Chem. Chem. Phys.*, **16**, 20347 (2014).
3. C. Wang, L. Su, N. Wang, D. Lv, D. Wang, J. Yang, and Y. Qian, *J. Mater. Chem. A*, **10**, 4060 (2022).
4. N. Wang, Y. NuLi, S. Su, J. Yang, and J. Wang, *J. Power Sources*, **341**, 219 (2017).
5. P. Padigi, G. Goncher, D. Evans, and R. Solanki, *J. Power Sources*, **273**, 460 (2015).
6. T. Schoetz, J. H. Xu, and R. J. Messinger, *ACS Appl. Energy Mater.*, **6**, 2845 (2023).
7. Z. Huang, X. Du, M. Ma, S. Wang, Y. Xie, Y. Meng, W. You, and L. Xiong, *ChemSusChem*, **16**, e202202358 (2023).
8. P. Saxena and P. Shukla, *Adv. Compos. Hybrid Mater.*, **4**, 8 (2021).
9. W. P. Kosar and S. Morris, *J. Coar. Technol. Res.*, **4**, 51 (2007).
10. W. Zhou, Y. Lin, K. Zou, C. Zhou, X. Gong, Y. Cao, and S. Jiang, *J. Mater. Sci., Mater. Electron.*, **32**, 28708 (2021).
11. H. Wang, Y. Bai, S. Chen, X. Luo, C. Wu, F. Wu, J. Lu, and K. Amine, *ACS Appl. Mater. Interfaces*, **7**, 80 (2015).
12. Y. Uemura, C. Y. Chen, Y. Hashimoto, T. Tsuda, H. Matsumoto, and S. Kuwabata, *ACS Appl. Energy Mater.*, **1**, 2269 (2018).
13. J. Smajic, A. Alazmi, and P. M. F. J. Costa, *MRS Adv.*, **4**, 807 (2019).
14. V. A. Elterman, P. Y. Shevelin, L. A. Yolshina, E. G. Vovkotrub, and A. V. Borozdin, *J. Mol. Liq.*, **320**, 114482 (2020).
15. D. Ma, D. Yuan, C. P. de León, Z. Jiang, X. Xia, and J. Pan, *Energy Environ. Mater.*, **6**, e12301 (2023).
16. L. L. Chen, N. Li, H. Shi, Y. Zhang, W. L. Song, S. Jiao, H. Chen, and D. Fang, *Nano Res.*, **13**, 419 (2020).
17. L. L. Chen, W. L. Song, N. Li, H. Jiao, X. Han, Y. Luo, M. Wang, H. Chen, S. Jiao, and D. Fang, *Adv. Mater.*, **32**, 2001212 (2020).
18. Restriction of per- and polyfluoroalkyl substances (PFAS) by the European Chemical Agency (ECHA), Bundesanstalt für Arbeitsschutz und Arbeitsmedizin Federal Institute of Occupational Safety and Health in Germany, https://baua.de/DE/Services/Presse/Pressemitteilungen/2023/02/pm08-23.html, 30.11.2023.
19. M. Angell, C. J. Pan, Y. Rong, C. Yuan, M. C. Lin, B. J. Hwang, and H. Dai, *PNAS*, **114**, 834 (2017).
20. S. Geetha and D. C. Trivedi, *Bull. Electrochem.*, **19**, 37 (2003).
21. D. M. Correia, C. M. Costa, E. Lizundia, R. S. I. Serra, J. A. Gómez-Tejedor, L. T. Biosca, J. M. Meseguer-Dueñas, J. L. G. Ribelles, and S. Lanceros-Méndez, *J. Phys. Chem. C*, **123**, 27917 (2019).
22. D. M. Correia, C. M. Costa, J. C. Rodríguez Hernández, I. Tort-Ausina, L. T. Biosca, C. T. Cabanilles, J. M. Meseguer-Dueñas, I. Krakovsky, S. Lanceros-Méndez, and J. L. Gómes Ribelles, *Cryst. Growth Des.*, **21**, 4406 (2021).
23. M. Malik, K. N. Ng, and G. Azimi, *Electrochim. Acta*, **354**, 136708 (2020).
24. P. Wasserscheid and W. Keim, *Angew. Chem. Int. Ed.*, **39**, 3772 (2000).
25. H. M. A. Abood, A. P. Abbott, A. D. Ballantyne, and K. S. Ryder, *Chem. Commun.*, **47**, 3523 (2011).
26. H. Jiao, C. Wang, J. Tu, D. Tian, and S. Jiao, *Chem. Common.*, **53**, 2331 (2017).
27. Y. Bormashenko, R. Pogreb, O. Stanevsky, and E. Bormashenko, *Polym. Test.*, **23**, 791 (2004).
28. Y. Peng and P. Wu, *Polymer*, **45**, 5295 (2004).
29. W. Li, H. Li, and Y. M. Zhang, *J. Mater. Sci.*, **44**, 2977 (2009).
30. A. JabbarniaR. Asmatulu, *J. Mater. Sci. Technol.*, **2**, 43 (2015).
31. N. Daems, S. Milis, R. Verbeke, A. Szymczyk, P. P. Pescarmona, and I. F. J. Vankelecom, *RSC Adv.*, **8**, 8813 (2018).
32. S. F. Kasbi, S. H. Jafari, H. A. Khonakdar, V. Goodarzi, and A. Torabi, *J. Appl. Polym. Sci.*, **137**, e49403 (2020).
33. P. Pendleton, B. Vincent, and M. L. Hair, *J. Colloid Interface Sci.*, **80**, 512 (1981).
34. C. Yie-Shun, J. Jagur-Grodzinski, and D. Vofsi, *J. Polym. Sci. Polym. Chem. Ed.*, **23**, 1193 (1985).
35. X. Xiao, Z. Zeng, and S. Xiao, *J. Hazard. Mater.*, **151**, 118 (2008).
36. K. S. Samra, S. Thakur, and L. Singh, *J. Lumin.*, **131**, 686 (2011).
37. O. A. Streletskiy, I. A. Zavidovskiy, I. F. Nuriahmetov, A. A. Khaidarov, A. V. Pavlikov, and K. F. Minnebaev, *J. Compos. Sci.*, **7**, 264 (2023).
38. M. Peltzer and C. Simoneau, Report of an interlaboratory comparison from the European Reference Laboratory for Food Contact: IL C002 2013—Identification of polymeric materials. EUR 26467. Luxembourg (Luxembourg): Publications Office of the European Union; 2013. JRC87373 https://doi.org/10.2788/6233.
39. Z. Yang, M. Guo, P. Meng, M. Jiang, X. Qiu, J. Zhang, and C. Fu, *Chem. Eur. J.*, **29**, e202203546 (2023).
40. B. Imtiaz, N. A. Shepelin, P. C. Sherrell, S. E. Kentish, and A. V. Ellis, *J. Membr. Sci.*, **632**, 119347 (2021).
41. H. Wang, Z. Liu, E. Wang, R. Yuan, D. Gao, X. Zhang, and Y. Zhu, *Appl. Surf. Sci.*, **332**, 518 (2015).
42. J. Sharma, C. Totee, V. Kulshrestha, and B. Ameduri, *Eur. Polym. J.*, **201**, 112580 (2023).
43. S. Thulasiraman, N. M. M. Yunus, P. Kumar, Z. R. Kesuma, N. Norhakim, C. D. Wilfred, T. M. Roffi, M. F. Hamdan, and Z. A. Burhanudin, *Materials*, **15**, 2818 (2022).
44. F. Liu, X. Zhong, J. Xu, Z. Wang, and Z. Shi, *J. Phys.: Conf. Ser.*, **1347**, 012109 (2019).
45. M. M. Ahmed, J. Hrůza, M. Stuchlík, V. Antoš, and J. Müllerová, *Eur. Polym. J.*, **156**, 110605 (2021).
46. B. Alenazi, A. Alsalme, S. G. Alshammari, R. A. Khan, and M. R. H. Siddiqui, *J. Chem.*, **2020**, 3894804 (2020).
47. T. Yoshioka, T. Kameda, S. Imai, M. Noritsune, and A. Okuwaki, *Polym. Degrad. Stab.*, **93**, 1979 (2008).
48. V. V. Korshak and Y. P. Kudryavtsev, *Makromol. Chem. Rapid Commun.*, **9**, 135 (1988).
49. W. Zhu, N. Hoshida, G. N. P. Jati, Y. Yoshida, K. Adachi, J. Zhu, M. Ihara, E. Marin, and G. Pezzotti, *Mater. Today Commun.*, **32**, 103884 (2022).
50. S. G. Khokarale, P. Jablonski, D. Nikjoo, V. M. Dinh, O. Sundman, K. Irgum, and J. P. Mikkola, *Sustain. Chem.*, **3**, 455 (2022).
51. O. A. Streletskiy, I. A. Zavidovskiy, O. Y. Nishchak, A. A. Khaidarov, N. F. Savchenko, and A. V. Pavlikov, *J. Exp. Theor. Phys.*, **135**, 844 (2022).
52. V. E. Zhivulin, D. A. Zherebtsov, S. M. Lebedeva, M. V. Shtenberg, A. A. Osipov, and L. A. Pesin, *Phys. Solid State*, **59**, 408 (2017).
53. C. S. Casari, A. Li Bassi, L. Ravagnan, C. Lenardi, P. Piseri, G. Bongiorno, C. E. Bottani, and P. Milani, *Phys. Rev. B*, **69**, 075422 (2014).
54. O. A. Streletskiy, I. A. Zavidovskiy, I. F. Nuriahmetov, O. Y. Nishchak, A. V. Pavlikov, and N. F. Savchenko, *C*, **9**, 82 (2023).
55. Y. G. Kryazhev, V. S. Solodovnichenko, N. V. Antonicheva, T. I. Gulyaeva, V. A. Drozdov, and V. A. Likholobov, *Prot. Met. Phys. Chem. Surf.*, **45**, 398 (2009).
56. H. Niino and A. Yabe, *J. Polym. Sci., Part A: Polym. Chem.*, **36**, 2483 (1998).
57. Q. Jin, L. Zhou, and H. Nasr-El-Din, *SPE J.*, **21**(03), 1050 (2016).

58. A. Bodor, I. Tóth, I. Bányai, Z. Szabó, and G. T. Hefter, *Inorg. Chem.*, **39**, 2530 (2000).
59. A. Cadiau, A. L. Bail, A. Hémon-Ribaud, M. Leblanc, M. Body, F. Fayon, E. Durand, J. C. Boulou, and V. Maisonneuve, *Cryst. Growth Des.*, **10**, 5159 (2010).
60. H. Yang et al., *Angew. Chem. Int. Ed.*, **57**, 1898 (2018).
61. S. Liu et al., *Nano Energy*, **66**, 104159 (2019).
62. M. C. Lin et al., *Nature*, **520**, 324 (2015).
63. G. A. Elia, I. Hase, G. Greco, T. Diemant, K. Marquardt, K. Hoeppner, R. J. Behm, A. Hoell, S. Passerini, and R. Hahn, *J. Mater. Chem. A*, **5**, 9682 (2017).
64. C. Mukundan, M. Eckert, and J. F. Drillet, *Batter. Supercaps*, **6**, e202300042 (2023).
65. M. C. Huang, C. H. Yang, C. C. Chaing, S. C. Chiu, Y. F. Chen, C. Y. Lin, L. Y. Wang, Y. L. Li, C. C. Yang, and W. S. Chang, *Energies*, **11**, 2760 (2018).
66. W. A. Appiah, M. P. Stockham, and J. M. Garcia Lastra, *Batteries & Supercaps*, **6**, e202300258 (2023).
67. J. Wei, W. Chen, D. Chen, and K. Yang, *J. Mater. Sci. Technol.*, **34**, 983 (2018).
68. Z. Yu, Y. Xie, W. Wang, J. Hong, and J. Ge, *Front. Chem.*, **11**, 1190102 (2023).
69. K. Matsumoto, K. Takagi, and R. Hagiwara, *J. Electrochem. Soc.*, **159**, H876 (2012).
70. K. Matsumoto, D. Minori, K. Takagi, and R. Hagiwara, *Carbon*, **67**, 434 (2014).
71. Q. Wang, D. Zheng, L. He, and X. Ren, *Phys. Rev. Applied*, **12**, 044060 (2019).
72. G. Wang, M. Yu, and X. Feng, *Chem. Soc. Rev.*, **50**, 2388 (2021), 2443.